



Polylactic Acid (PLA) Reinforced with Date Palm Sheath Fiber Bio-Composites: Evaluation of Fiber Density, Geometry, and Content on the Physical and Mechanical Properties

Said Awad, Tamer Hamouda, Mohamad Midani, Evina Katsou & Mizi Fan

To cite this article: Said Awad, Tamer Hamouda, Mohamad Midani, Evina Katsou & Mizi Fan (2023) Polylactic Acid (PLA) Reinforced with Date Palm Sheath Fiber Bio-Composites: Evaluation of Fiber Density, Geometry, and Content on the Physical and Mechanical Properties, Journal of Natural Fibers, 20:1, 2143979, DOI: [10.1080/15440478.2022.2143979](https://doi.org/10.1080/15440478.2022.2143979)

To link to this article: <https://doi.org/10.1080/15440478.2022.2143979>



© 2022 The Author(s). Published with license by Taylor & Francis Group, LLC.



Published online: 15 Nov 2022.



Submit your article to this journal [↗](#)



Article views: 729



View related articles [↗](#)



View Crossmark data [↗](#)

Poly(lactic Acid) (PLA) Reinforced with Date Palm Sheath Fiber Bio-Composites: Evaluation of Fiber Density, Geometry, and Content on the Physical and Mechanical Properties

Said Awad^a, Tamer Hamouda^b, Mohamad Midani^{id c}, Evina Katsou^{id a}, and Mizi Fan^a

^aDepartment of Civil and Environmental Engineering, College of Engineering, Design and Physical Sciences, Brunel University London, Uxbridge, UK; ^bTextile Research Division, National Research Centre, Cairo, Egypt; ^cWilson College of Textiles, NC State University, Raleigh, North Carolina, USA

ABSTRACT

Significant interest for utilizing and processing natural fibers (NF) to develop sustainable and fully biodegradable composites evolved as the global environmental concerns upsurge. Date palm tree (DPT) accounts for more than 2.8 million tons of waste annually, making it the most abundant agricultural biomass waste in the MENA region. This study investigates the effect of date palm fiber (DPF) density, diameter size and content on both the mechanical and physical properties of poly(lactic acid) (PLA) reinforced DPF bio-composite. The bio-composites are developed using melt-mixing technique which is followed by compression molding. The influence of the mechanical properties is investigated by evaluating the tensile, flexural and impact strengths. Meanwhile bio-composite thickness swelling (TS), moisture content (MC) and water absorption (WA) characteristics are evaluated. Bio-composite microstructures are examined using SEM to investigate the interfacial bonding between PLA matrix and DPF. Results showed that at 40 wt.% DPF, the TS, MC, and WA were the highest demonstrating an increase of 4.10%, 4.95%, and 8.22%, respectively. Although the results demonstrated a decrease in mechanical properties as DPF content increased (depending on DPF geometry), the results indicate that the developed technologies could be commercialized under the waste management scheme for non-structural applications.

摘要

随着全球环境问题的加剧,人们对利用和加工天然纤维(NF)开发可持续和完全生物降解的复合材料产生了极大的兴趣。椰枣树(DPT)每年产生280多万吨废弃物,是中东和北非地区最丰富的农业生物质废弃物。本研究研究了椰枣纤维(DPF)密度、直径大小和含量对聚乳酸(PLA)增强DPF生物复合材料力学和物理性能的影响。生物复合材料是使用熔融混合技术开发的,然后是压缩成型。通过评估拉伸、弯曲和冲击强度来研究力学性能的影响。同时,评估了生物复合材料的厚度膨胀(TS)、水分含量(MC)和吸水率(WA)特性。使用SEM检查生物复合材料微观结构,以研究PLA基质和DPF之间的界面结合。结果表明,在40重量%的DPF下,TS、MC和WA最高,分别增加了4.10%、4.95%和8.22%。尽管结果表明,随着DPF含量的增加(取决于DPF的几何形状),机械性能有所下降,但结果表明,开发的技术可以在非结构应用的废物管理计划下商业化。

KEYWORDS



PLA composites; date palm fibers; biodegradable composites; bio-composites; mechanical properties; physical properties

关键词

聚乳酸复合材料; 关键词; 椰枣纤维; 生物降解复合材料; 生物复合材料; 机械性能; 物理特性

Introduction

The growing environmental concerns and awareness along with the shortage of natural resources have urged for investigations on biodegradable composites as a substitute for non-biodegradable and

CONTACT Mizi Fan  mizi.fan@brunel.ac.uk  Department of Civil and Environmental Engineering, College of Engineering, Design and Physical Sciences, Brunel University London, Uxbridge UB8 3PH, UK

© 2022 The Author(s). Published with license by Taylor & Francis Group, LLC.

This is an Open Access article distributed under the terms of the Creative Commons Attribution License (<http://creativecommons.org/licenses/by/4.0/>), which permits unrestricted use, distribution, and reproduction in any medium, provided the original work is properly cited.

petroleum based composites (Dong et al. 2014; Siakeng et al. 2020). A variety of biodegradable polymers (biopolymers) such as polyhydroxyalkanoates (PHA), polylactic acid (PLA), and polybutylene succinate (PBS) have been reported by researchers on their performance to be used as a matrix system to develop biodegradable composites (Foruzanmehr et al. 2016; Huda et al. 2008). These biopolymers are naturally obtained and can be combined with various natural materials such as natural plant fibers (NF) to produce biodegradable composites with enhanced characteristics (Jia, Gong, and Paul 2014). Among other biopolymers discussed, PLA is reported to be the most commercially utilized matrix system that has demonstrated promising results for developing sustainable composite as a substitute to synthetic polymers (Debeli, Qin, and Guo 2018; Del Campo et al. 2022). The high cost of biopolymers compared to synthetic or petroleum-based plastics does not encourage industries to utilize biopolymers unless forced by governmental regulations (Said et al. 2020).

The agricultural sectors generate enormous amounts of agro-waste annually. Globally, the lignocellulosic residues alone exceed 600 million tons annually and are poorly managed. Recycling NF by incorporating them into composites to manufacture renewable and biodegradable materials have drawn considerable attention due to several factors such as low cost, low density, biodegradability, availability, absence of associated health hazards, and they are relatively non-abrasive (Alsaeed, Yousif, and Ku 2013; Aly et al. 2021; Herrera-Franco and Valadez-González 2004; Puglia, Biagiotti, and Kenny 2004) and can help in waste reduction and reduce the cost of the composites developed (Madurwar, Ralegaonkar, and Mandavgane 2013). It is conceivable that a certain type of plant fibres are more attractive for each region. DPF are considered as the most abundant agricultural biomass waste in the MENA region yielding more than 2.8 million tons annually (Awad et al. 2020; Elseify et al. 2019). This waste is either incinerated or deposited into landfills causing serious environmental pollution as well as death of important soil microorganisms (Ahmad, Hamed, and Al-Kaabi 2009; Awad et al. 2020; Hamouda and Aly 2020). Thus, investigating an industrial application that can utilize this huge amount of biomass waste can be within the waste management scheme that are being implemented by most of the countries. However, the utilization of DPF raises difficulties, as is the case with all plant fibres. The hydrophilic polar nature of the lignocellulosic fibres makes it difficult to achieve proper adhesion to hydrophobic polymers. This is because of the abundance of hydroxyl groups that provide the fibre with a high affinity to water, hindering proper wetting of the fibres by nonpolar polymers. Several researches have been conducted to improve the compatibility of natural fibres with polymers. This was successfully achieved by treating the DPF either physically or chemically (Amirou et al. 2013; Awad et al. 2020; Elseify et al. 2020; Lahouioui et al. 2019; Oushabi et al. 2017; Ozerkan et al. 2013; Taha, Steuernagel, and Ziegmann 2006) or by using coupling agents as reported by several researchers which increases the adhesion between NF and polymer matrix (Hamouda and Hassanin 2020; Hamouda et al. 2017; Hassanin et al. 2016; Matuana et al. 1998; Mittal, Saini, and Sinha 2016; Pickering et al. 2007; Zhou, Cheng, and Jiang 2014). However, a critical aspect of understanding the geometry, length and diameter, of NF and in specific DPF, has not yet been investigated in depth and there is a lack in consistency on their effect as a reinforcement in polymeric composites.

This study presents an investigation on the effect of DPF density, geometry and content on the physical, and mechanical properties of PLA/DPF bio-composites fabricated by melt-mixing and compression molding processing techniques. The thickness swelling (TS), moisture content (MC), water absorption (WA), tensile strength, flexural strength, and impact strength of four different fiber contents (10, 20, 30, and 40) wt.% and six different fiber diameters (Unsieved, $\geq 1,000 \mu\text{m}$, 500–1,000 μm , 250–500 μm , 125–250 μm , and $\leq 125 \mu\text{m}$) are evaluated. To our current knowledge, such holistic study has not been comprehended on developing 100% biodegradable DPF bio-composites. Thus, it is expected that this study can shed the light on the commercialization of PLA/DPF bio-composites in a more comprehensive approach producing 100% biodegradable composites.

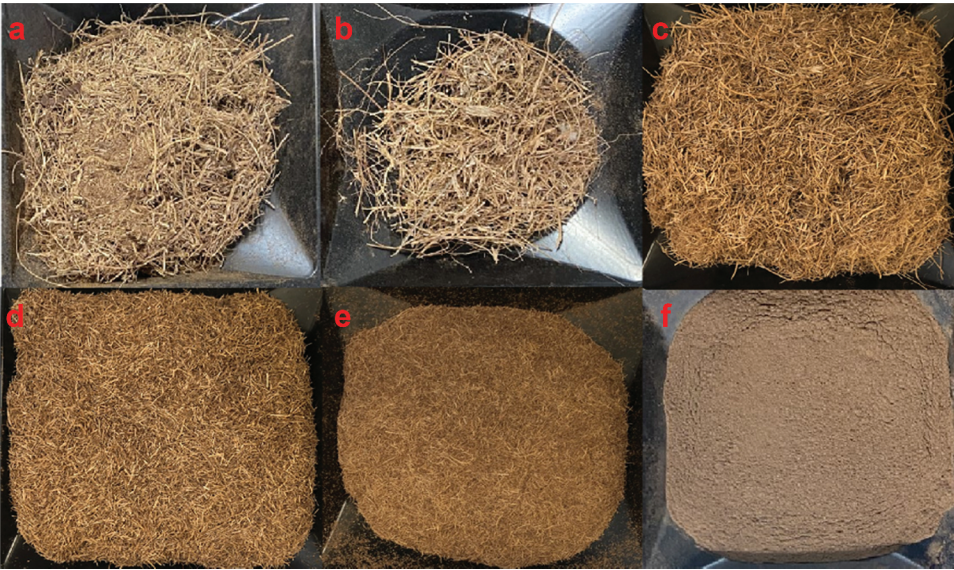


Figure 1. Shows different sieved size of DPF – (a) unsieved DPF, (b) $\geq 1000 \mu\text{m}$ DPF, (c) $500\text{--}1,000 \mu\text{m}$ DPF, (d) $250\text{--}500 \mu\text{m}$ DPF, (e) $125\text{--}250 \mu\text{m}$ DPF, (f) $\leq 125 \mu\text{m}$ DPF (Awad et al. 2021).

Materials and methods

Materials

Raw DPF sheath surrounding the date palm stem, were supplied by Valorizen Research and Innovation Centre, Egypt. DPF were washed with distilled water and then dried in an oven at 60°C for 24 hours and then grinded using Retsch cutting mill (SM 100, Germany) equipped with a 2 mm sieve. The grinded DPF were sieved through several mesh sizes $1,000 \mu\text{m}$, $500 \mu\text{m}$, $250 \mu\text{m}$, and $125 \mu\text{m}$ (Figure 1), and then preserved in sealed polythene bags. Furthermore, PLA, polymer matrix, was obtained from Ecodeck Ltd, UK, in pellet form. The pellets were dried in an oven at 60°C for 24 hours.

Processing of DPF/PLA bio-composite

The DPF and PLA polymer matrix were processed in a Barbender Plastograph twin-screw mixer (with Cam blades for mixer type N50EHT) at 170°C and 50 rpm for 6 minutes. Samples with four different mass proportions and six different fiber diameter size were produced. This was achieved by initially feeding into the mixer the required amount of PLA pellets for each batch allowing it to completely melt for 3 minutes, and subsequently feeding in the DPF for 3 minutes to obtain a uniform mixture. Thus, the resulted mixture was grinded to pellets using Retsch cutting mill (SM 100, Germany) equipped with a 2 mm sieve. The grinded pellets were compression molded into a $100 \text{ mm (L)} \times 100 \text{ mm (W)} \times 40 \text{ mm (T)}$ mould using an electrically heated hydraulic press. Compression molding procedure involved pre-heating at 170°C for 10 minutes without applied load followed by 5 minutes compressing at the same temperature under 10 MPa weight, and subsequently cooling under load until the mould reached 35°C . The compression molded composite were then cut into $100 \text{ mm (L)} \times 10 \text{ mm (W)} \times 4 \text{ mm (T)}$ samples to be tested for physical and mechanical properties. Figure 2 demonstrates a schematic diagram on the processing of DPF/PLA composite.

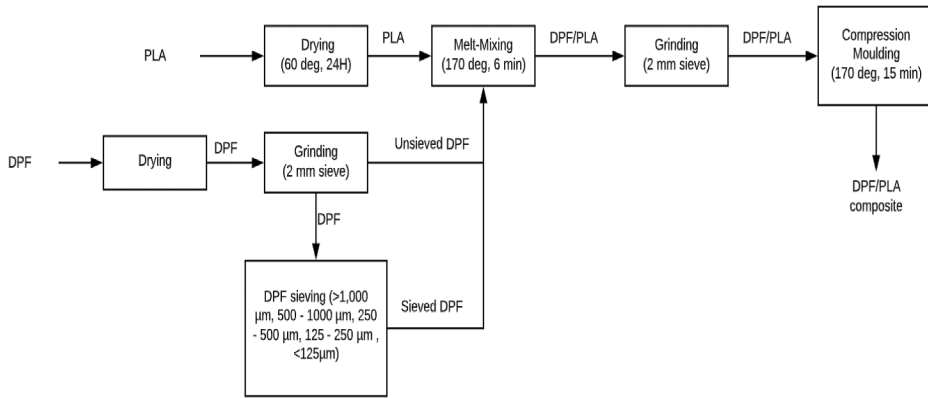


Figure 2. Schematic diagram on processing of DPF/PLA composite.

Physical property analysis

Density

The density was calculated for DPF/PLA bio-composite using AccuPyc II 1340 gas pycnometer with temperature control and a 100 cm³ chamber volume. The samples were weighed directly into the chamber cup using a measuring balance with 0.01 g accuracy. Helium was admitted into the compartment until reaching an equilibrium rate of 0.0050 psig/min. The samples were tested for 10 purge and 10 cycles to increase the accuracy of the test. Theoretical density was calculated as shown in Equation (1) where ρ_c is the theoretical density of the composite, ρ_f is the density of fiber (DPF), V_f is the volume fraction of the fiber (DPF), ρ_m is the density of the polymer matrix (PLA), and V_m is the volume fraction of polymer matrix (PLA). The volume fraction percentage of voids (V_v) in the composites is calculated as shown in Equation (2) where ρ_t is the theoretical density and ρ_e is the experimental density of the composite (Swain and Biswas 2013).

$$\rho_c = \rho_f V_f + \rho_m V_m \quad (1)$$

$$V_v = \frac{\rho_t - \rho_e}{\rho_t} \quad (2)$$

Thickness swelling (TS)

Thickness swelling of the fabricated samples were determined according to BS EN 317, where samples were immersed in a water bath at (20 ± 1)^oC for 24 hours. The samples thickness was measured before and after 24 h water immersion. Equation 3 demonstrates the calculation of thickness swelling, where TS is the thickness swelling of the composite, t_2 is the thickness of the composite before immersion in water bath in millimeters, and t_1 is the thickness of the composite after immersion in water bath in millimeters. The nominated dimensions of the specimens were 10 mm (L) x 10 mm (W) x 4 mm (T).

$$TS = \frac{t_2 - t_1}{t_1} \times 100 \quad (3)$$

Moisture content (MC) and water absorption (WA)

The moisture content of the samples fabricated was determined according to BS EN 322 as shown in equation 4, where MC is the moisture content, M_f is the initial mass of the composite before drying measured in grams and M_i is the mass of the composite after drying which is measured in grams. The mass of the samples was recorded to an accuracy of 0.01 g. The sample was then oven dried at (103 ±

2)°C until a constant weight is reached. Afterwards the samples were weighted using a measuring balance with 0.01 g accuracy. For water absorption evaluation, samples were immersed in a water bath at $(20 \pm 1)^\circ\text{C}$ for 24 hours. Equation (5) demonstrates the calculation of water absorption, where WA is the water absorption of the composite, M_2 is the mass of the composite after immersion in water bath in grams, and M_1 is the mass of the composite before immersion in water bath in grams. The samples were weighted before and after immersing in the water bath. Moreover, the dimensions of the specimens were 10 mm (L) x 10 mm (W) x 4 mm (T).

$$\text{MC} = \frac{M_f - M_i}{M_i} \times 100 \quad (4)$$

$$\text{WA} = \frac{M_2 - M_1}{M_1} \times 100 \quad (5)$$

Mechanical property analysis

The mechanical properties of the developed composites were measured at 25°C and relative humidity of 60% determined according to BS EN ISO 14125:1998 and BS EN ISO 527-2:2012 for flexural and tensile strength, respectively. Flexural (3 point bending test) and tensile strength tests were conducted using an Instron 5900 testing machine with a load cell capacity of 30 kN and speed of 1 mm/min. Charpy notched impact test was done according to ISO 179-1:2010 using CEAST Torino 6546/000 with an edgewise impact and 2J hammer capacity. The dimensions of the specimens tested for mechanical properties were 100 mm (L) x 10 mm (W) x 4 mm (T). For each sample, the flexural, tensile and impact properties are the average of five measurements.

Microstructure analysis

Scanning Electron Microscope (SEM), TESCAN-VEGA 3 (Czech Republic) field emission was used to examine the microstructure of the composites developed to ensure the homogeneous mixture between the DPFs and PLA, and study the failure mechanism due to different sieving sizes. Samples are obtained by sticking the samples on a carbon adhesive tape. Afterwards, the samples are coated with a thin layer of gold film using Edwards S 150B sputter coater to provide electrical conductivity. Following coating, samples were observed and operated with 30 kV coupled with an Energy Dispersive X-rays (EDX) analyzer unit.

Results and discussion

Effect of DPF geometry and loading content on the physical properties

Particle size and density analysis of DPF and its bio-composite

Evaluating the particle size distribution of DPF that can be used as a reinforcement for developing sustainable bio-composites is crucial. DPF content passing through various sieve sizes was evaluated as shown in Figure 3. Figure 3 demonstrates that DPF particle size from the sheath of DPT are mainly 250–500 μm , where 94% of grinded DPF passed through 1,000 μm sieve, where 15% got retained on the 500 μm sieve and the rest, 79% passed through. Afterwards, 56% of DPF retained on the 250 μm sieve in which only 23% passes through having 16% retaining on the 125 μm sieve and the remaining 7% passed through. Moreover, it was observed that DPF caused sieve clogging which might had led to misleading results. Also, trying to calculate and evaluating the length of DPF for each sieve size is very crucial where the aspect ratio can be derived. However, due to the non-uniform diameter and length of DPF the variance is very high and this will lead to a misrepresentation of accurate results. Thus, it is

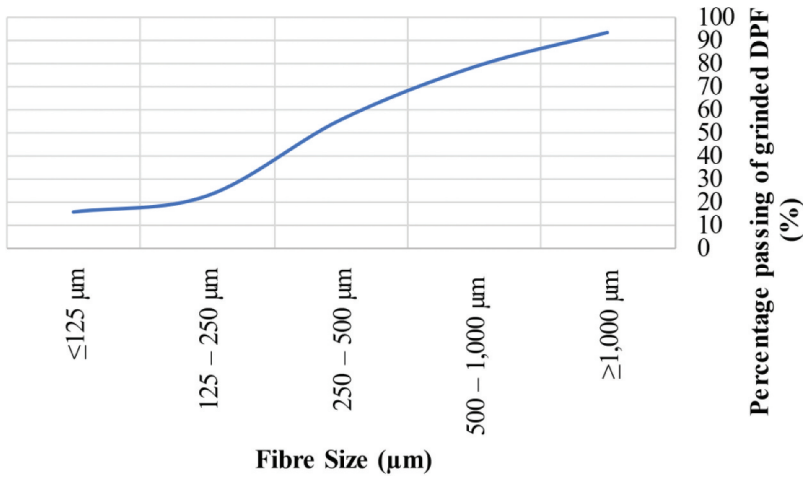


Figure 3. Particle distribution of sieved DPF.

difficult to calculate the real value of length and diameter of DPF to derive the real particle size distribution.

The density of PLA was experimentally evaluated to be 1.178 g/cm³. The bulk density of various DPF sieve size were reported in previous work to evaluate the difference in volume of each sieve size having the same wt.% loading (Table 1). The bulk density is higher for DPF size of ≤125 µm compared to 125–500 µm and then density decreased as the DPF diameter size increased. This is also reflected in the density of their corresponding fabricated composites which were evaluated and predicted as shown in Table 2. The decrease in density can be due to insufficient PLA matrix to blend with the DPF of low density, ≤125 µm and ≥1,000 µm, due to the high volume of DPF available. This may lead to a direct influence on the structure of the composite, which in turn affects the physical and mechanical characteristics of the composite. Additionally, the manufacturing process parameters such as temperature and mixing time have a great influence on the physical and mechanical properties of the bio-composites developed due to the formation of high voids resulting from the air entrapment which can affect the density of the bio-composites (Radzi et al. 2019).

The difference between the experimental and theoretical densities of the bio-composites developed can provide an indication on the volume fraction percentage of voids (Vv %) in the composites. As the Vv % increases within the bio-composites a weaker interface strength due to inadequate adhesion between DPF and PLA which results in crack initiation and growth leading to a reduction in strength of the composite. Also, the Vv% gives an indication of the physical properties where the WA can be directly proportional related to the Vv%. It is observed (Table 3) that ≤125 µm at 40 wt.% loading content had the highest Vv of 21.72% which can be correlated to the findings of the physical and mechanical tests of the composites where the same DPF size and loading had the highest WA%

Table 1. PLA and DPF sieve size densities.

Material	Density (g/cm ³)	Reference
PLA	1.178	This study
≤125 µm	0.4079	(Awad et al. 2021)
125–250 µm	0.5024	
250–500 µm	0.4762	
500–1,000 µm	0.4413	
≥1,000 µm	0.3317	
Unsieved	0.4658	

Table 2. DPF/PLA bio-composite theoretical and experimental densities at different DPF loading content (Wt.%).

DPF size (μm)	Theoretical density (g/cm^3)				Experimental density (g/cm^3)			
	10% DPF	20% DPF	30% DPF	40% DPF	10% DPF	20% DPF	30% DPF	40% DPF
≤ 125	0.99	0.86	0.75	0.67	0.98	0.84	0.72	0.52
125–250	1.04	0.93	0.84	0.77	1.03	0.89	0.80	0.63
250–500	1.03	0.91	0.82	0.74	1.01	0.87	0.77	0.64
500–1,000	1.01	0.88	0.78	0.71	0.99	0.83	0.73	0.61
$\geq 1,000$	0.94	0.78	0.68	0.58	0.92	0.75	0.62	0.50
Unsieved	1.02	0.90	0.81	0.73	0.96	0.80	0.70	0.61

Table 3. Volume fraction percentage of voids (V_v) in DPF/PLA bio-composite.

DPF size (μm)	V_v (%) at different DPF loading contents (Wt.%)			
	10% DPF	20% DPF	30% DPF	40% DPF
≤ 125	0.97	2.32	3.73	21.72
125–250	1.26	3.83	5.24	17.72
250–500	2.00	3.91	5.96	13.15
500–1,000	2.22	5.19	6.92	13.93
$\geq 1,000$	2.05	4.28	8.13	13.56
Unsieved	5.61	11.27	13.76	16.98

content. Also, it can be deduced that as the DPF loading increased the V_v % increase in the composite which directly influences both the physical and mechanical properties negatively.

Thickness swelling of DPF/PLA bio-composites

Thickness swelling (TS) of the composites were examined for 48 hours to determine the dimensional stability of DPF composite which will aid in identifying its end use. It is directly related to the density, presence of voids (V_v %), and the interfacial bonding between the fiber and matrix (Awad et al. 2021). The results revealed that all samples reached the max TS% after 24 hours and no further increase in thickness was recorded afterward, presuming that the DPFs have reached maximum saturation and the voids within the composite may fully be filled with water. Table 4 and Figure 4 present the percentage increase in TS% for various DPF sieve size at different loading content. Pure PLA has the lowest TS, 0.06%, which is due to hydrophobic characteristics. The increase in DPF content causes an increase in TS% of the bio-composites developed. Thus, DPF/PLA bio-composites reinforced with 40 wt.% DPF contributed to the highest TS which also corresponds to the highest WA. The increase in the hydroxyl group with the increase of DPF where the swelling of the fibers will push the polymer matrix (PLA) to expand forming internal stresses within the bio-composite resulting in delamination between the DPF and PLA as shown in Figure 12. Also, the dispersion of the DPF may be reduced at high fiber volume fractions, resulting in an increase in the porosity of the composite, which leads to an increase in water uptake and thus composite thickness swelling. This phenomena was also observed in previous work reported on the effect of DPF as reinforcement for recycled polyvinyl chloride composites (Awad et al. 2021).

Table 4. Increase in TS% for various DPF sizes at different loadings (%).

Sieve Size (μm)	% Increase in TS by the increase of DPF loading (wt.%)		
	20% DPF	30% DPF	40% DPF
≤ 125	83.12	135.88	410.43
125–250	74.74	120.92	355.301
250–500	77.50	106.35	154.76
500–1,000	148.38	166.21	324.49
$\geq 1,000$	256.27	184.71	346.22
Unsieved	41.24	73.15	157.08

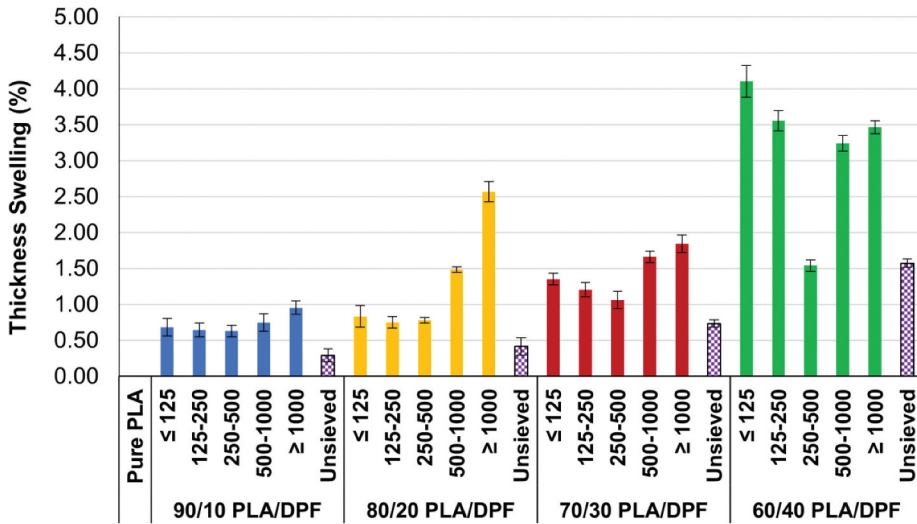


Figure 4. Effect of DPF geometry and loading on TS% of DPF/PLA composite.

Moisture content and water absorption of DPF/PLA bio-composites

The moisture content (MC) for DPF/PLA bio-composites after 48 hours are shown in Figure 5. Overall the composites with high DPF content, exhibit higher MC%, which is a common phenomenon to WA% and TS% due to the hydrophilic nature of DPF. However, the effect of DPF density and geometry on MC of the bio-composite varies depending on the DPF weight content. At a low loading content, an increasing trend in MC is observed as the DPF size increase from $\leq 125 \mu\text{m}$ to $\geq 1,000 \mu\text{m}$ at 10–30 wt.% loading content which is followed by a decrease in MC for unsieved DPF bio-composites. As the DPF diameter increased, the morphology of the DPF changes from powder to a needle-like shape which may develop voids that can be filled with water. Additionally, some of the DPF may be pulled out during the sample cutting, leaving a cavity that can allow water to be absorbed. Furthermore, $\leq 125 \mu\text{m}$ DPF sieve size has a larger surface area, which may result in a high adherence force between the DPF and PLA matrix, preventing water absorption. Consequently, at larger DPF diameter, water may be absorbed more due to the capillary system where larger DPF diameter is

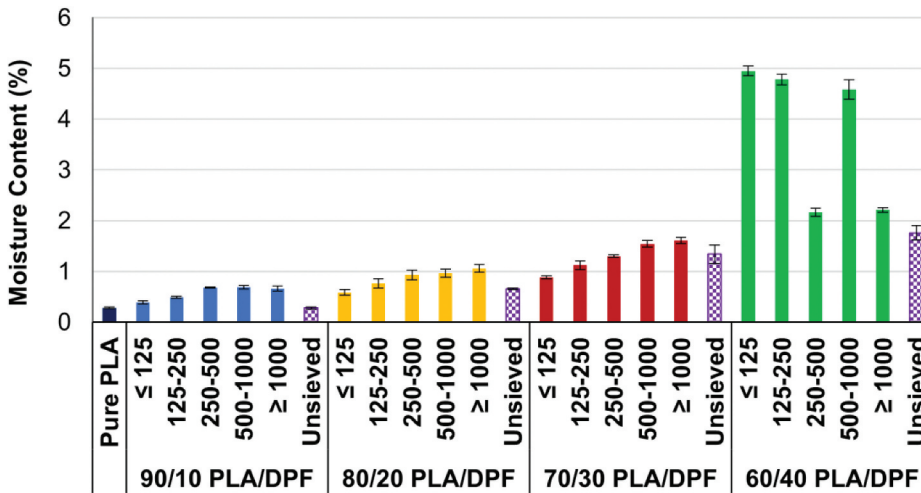


Figure 5. Effect of DPF geometry and loading on MC% of DPF/PLA composite.

composed of bundle of fibrils with longitudinal space between them causing water to be absorbed. At a high loading content, a significant increase in MC of $\leq 125 \mu\text{m}$, 125–250 μm , and 500–1,000 μm DPF size was observed. This may be an attribute which is related to the density of the fiber and having insufficient PLA matrix for homogenous bio-composite fabrication.

Table 5 shows the percentage increase in MC percent for different DPF sieve sizes at various loading content levels. The findings reveal that sieve size has a significant impact on the percentage increase in MC% at various weight contents. The most significant increase in MC% occurred when the loading content of $\leq 125 \mu\text{m}$ DPF sieve size increased from 30 to 40 wt.% which could possibly be due to the large volume of DPF present at high loading for low sieve size, $\leq 125 \mu\text{m}$, and low density, resulting in insufficient PLA matrix to produce a homogeneous perfectly compounded mix. As a result, there will be a weak interface between the polymer and the fiber, resulting in more voids within the composite and an increase in MC%.

Moreover, the WA% of the DPF reinforced PLA bio-composites was conducted to determine the amount of water absorbed under specified conditions for 24 hours. The importance of understanding the WA of the composites developed is to determine their end uses. Table 6 and Figure 6 demonstrates the increase in WA% for various DPF sieve sizes at different weight content and WA% for the bio-composites developed, respectively. Results demonstrated that the WA% of pure PLA composites was very low which reached 0.32% after 24 hours. It has been reported that although PLA is hydrophobic, the WA mainly occurred due to some voids formed within the composite while processing the composite. The DPF/PLA bio-composites showed an increase in WA% as the DPF content increased which follows the same trend as the TS% and MC% of the bio-composites developed. Thus, WA was maximum for composites with 40 wt.% DPF content (Figure 5). This increase in WA along with the increase of DPF content may be directly correlated to the hydrophilic nature of DPF (presence of hydroxyl group) which causes a OH-DPF interaction responsible for the WA% in the composites since PLA absorb minimal amount of water (Shakeri and Ghasemian 2010). Also, because DPF has a high porosity, a higher DPF content causes more water to be absorbed, resulting in an increase in the bio-composite's weight.

Moreover, the bio-composites reinforced with unsieved DPF showed the highest WA% at loading contents 10–30 wt.%, where WA% increased from 2.39% to 5.52% as the DPF loading content increased from 10 to 30 wt.%. This can be attributed to the high Vv% present which increases the tendency to absorb water within the capillary system. Also, he variable range of DPF sizes available

Table 5. Increase in MC% for various DPF sizes at different loadings (%).

Sieve Size (μm)	% Increase in MC by the increase of DPF loading (wt.%)		
	20% DPF	30% DPF	40% DPF
≤ 125	107.14	214.29	1667.90
125–250	171.59	300.02	1607.10
250–500	231.47	364.35	670.68
500–1,000	244.03	450.03	1536.50
$\geq 1,000$	277.85	473.73	688.86
Unsieved	134.84	377.53	527.37

Table 6. Increase in WA% for various DPF sizes at different loadings (%).

Sieve Size (μm)	% Increase in WA by the increase of DPF loading (wt.%)		
	20% DPF	30% DPF	40% DPF
≤ 125	260.02	412.10	2451.22
125–250	422.83	598.31	2345.63
250–500	440.03	714.16	1519.01
500–1,000	589.01	827.98	1652.34
$\geq 1,000$	467.96	1020.40	1610.50
Unsieved	1265.30	1611.91	2292.99

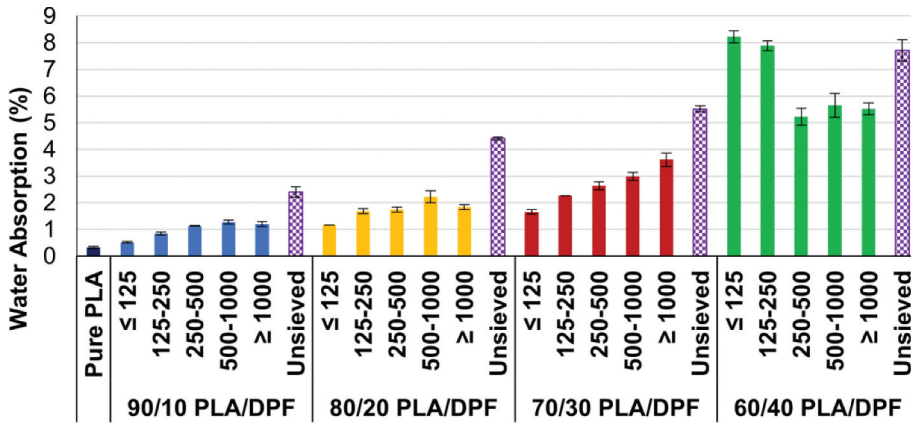


Figure 6. Effect of DPF geometry and loading on WA% of DPF/PLA composite.

reduces interfacial bonding with the polymer matrix, resulting in more voids within the bio-composite and a higher tendency to absorb water. Moreover, all bio-composites with $\leq 125 \mu\text{m}$ DPF recorded the lowest WA%, MC% and TS% at loadings 10–30 wt.%, which may be attributed to better interfacial bonding between DPF and PLA matrix system due to a better homogenous compounding, thus more DPF surface area being covered with the PLA matrix during compounding and lower voids present in the composite developed. This can also be justified by looking at the tensile strength of the composites developed where $\leq 125 \mu\text{m}$ DPF sieve size reinforcement at loading 10–30 wt.% showed the optimum tensile strength. However, at a loading content of 40 wt.%, $\leq 125 \mu\text{m}$ DPF sieve size shows a significant increase in WA%, 2451%. This can be attributed that at 40 wt.%, DPF with low sieve size and low density requires large volume of sample, and the PLA matrix is not enough to produce a homogenous perfectly compounded mix. As a result, a weak interface between PLA and DPF will exist, resulting in more voids within the bio-composite, requiring an increase in WA% to fill the voids to reach saturation. This is also demonstrated by the mechanical strength of the bio-composites developed, with the $\leq 125 \mu\text{m}$ DPF sieve size at 40% DPF content showing the lowest strength, which is due to the weak interfacial bonding between DPF and PLA.

Observations on the physical properties of DPF/PLA bio-composites developed show that the TS, MC, and WA % increased as the DPF content increased. This could be due to an increase in DPF volume fraction, which allows more water to be absorbed by DPF due to their hydrophilic nature, causing fiber swelling, which pushes the matrix and creates voids, weakening the interfacial bonding, and thus increasing the WA and TS of the bio-composite. Furthermore, different DPF diameters have different bulk densities, which could have a direct impact on the volume fraction of DPF added to bio-composites at the same content (wt. %), implying a direct impact on the physical properties of the developed bio-composites.

Effect of DPF geometries and loading content on the mechanical properties of DPF bio-composites

Flexural strength

DPF/PLA composites showed that the flexural strength was the lowest at $\leq 125 \mu\text{m}$ at all DPF loading content as shown in Figure 7. The unsieved DPF showed the highest reinforced strength at all loading content. This may be an attribute that the $\leq 125 \mu\text{m}$ DPF available in the unsieved DPF composite may be able to fill the voids around the larger fiber size, making the composites more compact. The decrease in flexural strength with the DPF size may be due to less compact interface structure, and the increase in the strength of composites with DPF from 500–1,000 μm and $\geq 1,000 \mu\text{m}$ may be attributed to the higher self-strength of the longer DPF than shorter DPF.

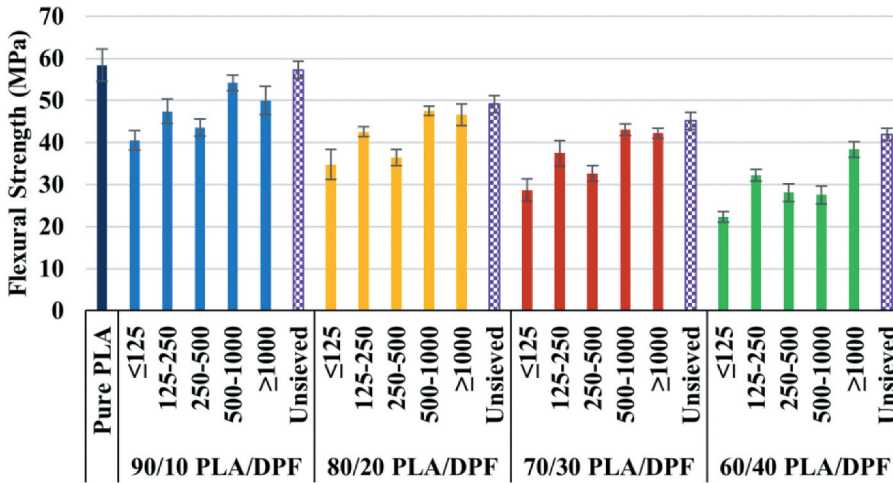


Figure 7. Effect of DPF geometry and loading content on flexural strength of DPF/PLA bio-composite.

It is most interesting that the flexural modulus of the bio-composites developed showed enhancement at specific DPF content and fiber geometry size as demonstrated in Figure 8. The addition of unsieved DPF, 125–250 μm DPF, 500–1,000 μm DPF, and ≥1,000 μm DPF as a reinforcement showed enhancement in the flexural modulus as the content increased from 10 to 30 wt.% then decreased at 40 wt.% content. The decrease observed at 40 wt.% may be an attribute that the volume fraction of the fiber is very high where there is not enough PLA matrix to develop a homogenous mix which resulted in high void fraction formation as demonstrated in Table 4. Moreover, the addition of ≤125 μm DPF showed no enhancement in the flexural modulus and decreased as the content of DPF increased. DPF with small geometrical size has a very low aspect ratio where the DPF are in powder form and there is no fiber length that can resist any stress or load applied to the composite.

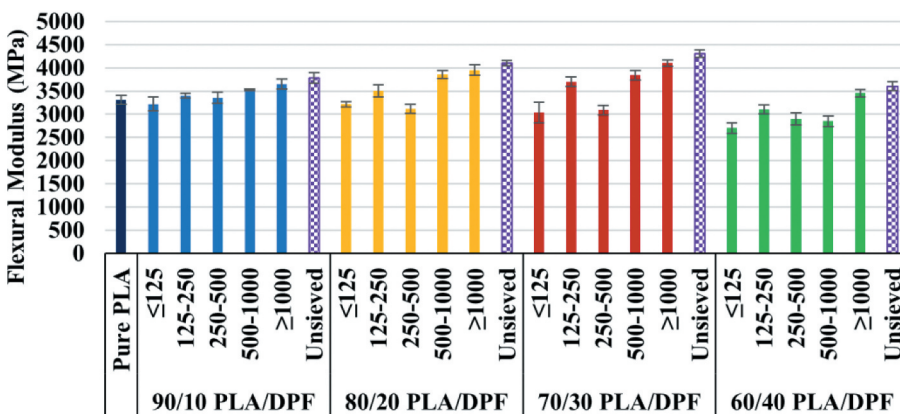


Figure 8. Effect of DPF geometry and loading content on the flexural modulus of DPF/PLA bio-composite.

Tensile strength

DPF geometry and content effect on DPF/PLA bio-composite tensile strength and Young's Modulus are presented in [Figures 9 and 11](#), respectively. The addition of DPF with varies DPF size and content led to a decrease in both the tensile strength and Young's Modulus of the bio-composites developed. The decrease in tensile strength with the increase in DPF loading has also been reported by other researchers (Awad et al. 2021; Rana, Mandal, and Bandyopadhyay 2003; Thwe and Liao 2002).

[Figure 5](#) shows that at a low loading content, 10–20 wt.%, 500–1,000 μm sieve size accounted to have the highest tensile strength which may be attributed to better interfacial bonding between DPF and PLA matrix system due to a better homogenous compounding and more polymer impregnating

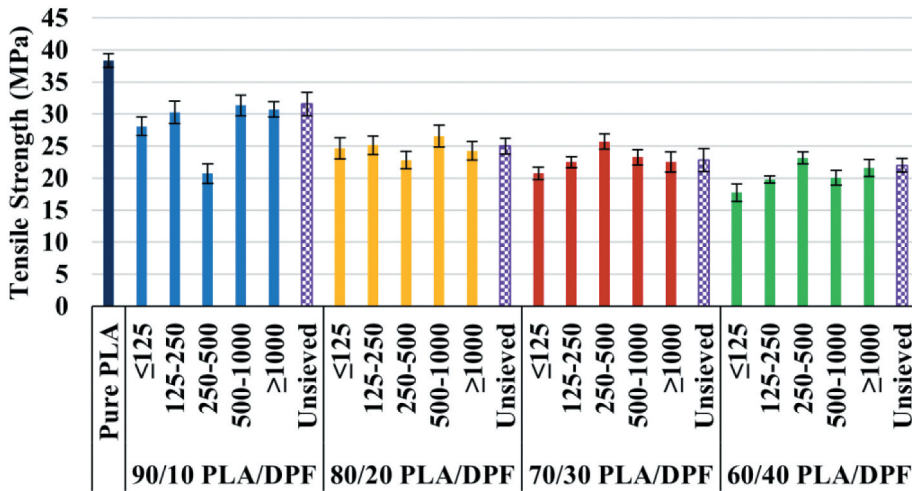


Figure 9. Effect of DPF geometry and loading content on tensile strength of DPF/PLA bio-composite.

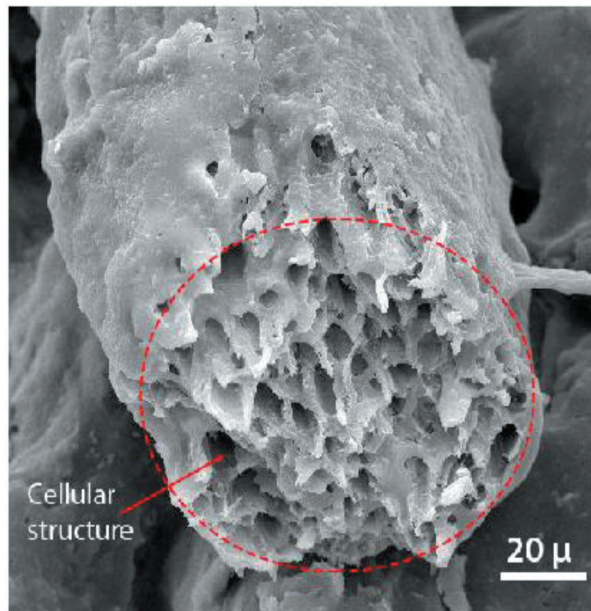


Figure 10. SEM image of the cellular structure of DPF [24].

through the fiber, thus more DPF surface area being covered with the PLA matrix during compounding forming a more compacted composite. Meanwhile, at a higher loading content, 30–40 wt.%, 250–500 μm sieve size accounted to have the highest tensile strength and $\leq 125 \mu\text{m}$ sieve size results showed to have the lowest tensile strength at all loading contents which may be considered as the critical DPF diameter for high DPF loading. The decrease in strength at $\leq 125 \mu\text{m}$ sieve size might be an attribute to the low density of DPF which has a high volume at a high loading weight content where there will not be enough PLA to form a homogeneously mixed bio-composite, thus creating more voids within the composite leading to a weaker interfacial bond that will reduce the tensile strength.

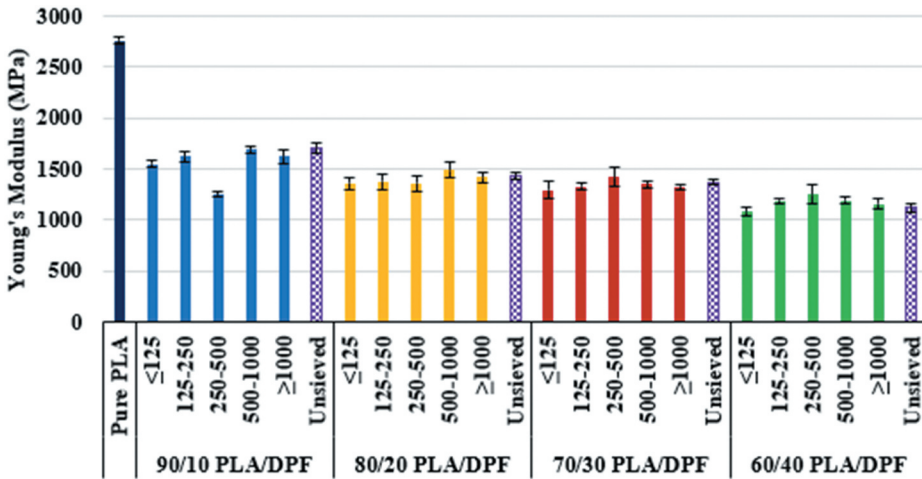


Figure 11. Effect of DPF geometry and loading content on Young's modulus of DPF/PLA bio-composite.

The stiffness, Young's Modulus, of the bio-composites developed decreased with increasing the loading content of DPF as shown in Figure 11. DPF utilized in this study are very ductile and characterized by high elongation at break and low modulus of elasticity as reported in (Awad et al. 2020). Such phenomena has been previously reported by several research work (Abdal-Hay et al. 2012; Rao and Rao 2007; Tahri et al. 2016). This phenomena is very similar to the behavior of the coconut coir fiber, with tensile modulus ranging from 2.0 to 8.0 GPa and elongation 15–51% (Adeniyi et al. 2019). This high extensibility in the fiber under tensile loading is attributed to the cellular structure of the fiber shown in Figure 10, which results in much lower resistance to lateral contraction and hence lower stiffness in axial direction during loading. Such low fiber stiffness results in a composite with low elastic modulus.

Impact strength

The toughness of the composites developed were measured using a Charpy notched impact test method, and results are demonstrated in Figure 12. Overall, the impact strength of the composites developed decreased with the increase in DPF loading content. The results clearly demonstrate poor-energy absorbing capabilities of the DPF reinforced composites, which can be discussed by addressing two mechanisms where DPF can decrease the impact strength of the composite. The first mechanism is the prevention of deformation and ductile mobility of polymer molecules as DPF, resulting in a decrease in the ability of the developed reinforced composites to absorb energy during crack propagation. The second mechanism involves DPF induced stress concentrations, formed by the agglomerations of DPF, that required less energy to initiate a crack. Such regions might occur at area of weak interfacial bonding, DPF ends, and regions where DPF contact each other, which aids in

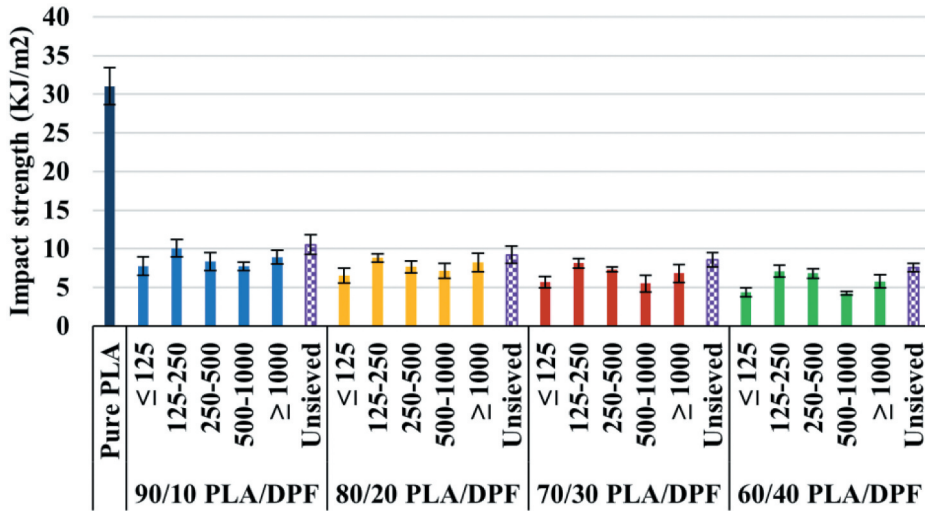


Figure 12. Effect of DPF geometry and loading content on impact strength of DPF/PLA bio-composite.

creating voids within the developed composite that requires low energy for crack initiation (Abdul Khalil et al. 2007; Trotignon et al. 1982). The results shown in Figure 12 DPF/PLA bio-composites showed that the optimal impact strength was achieved for the unsieved DPF at all DPF loading content, having a maximum impact strength of 10.52 KJ/m^2 at 10 wt.% DPF loading content.

Benchmarking DPF/PLA composites

Several researchers aimed to utilize DPF from various parts of DPT as a reinforcement in developing composites. A comparative study on the effect of DPF mesh as reinforcement using various polymeric matrices was investigated by many researchers as shown in Table 7. Aldousiri and his colleagues investigated DPF mesh as a reinforcement for recycled high-density polyethylene (R-HDPE). Results demonstrated that treated DPF shows enhanced mechanical properties for composite development (Aldousiri et al. 2013). Moreover, Saleh and his colleagues investigated developed bio-composites using thermoplastic starch (TPS) reinforced with DPF. Results showed that at 50 wt.% loading content of DPF increased the flexural and fatigue strength but no endurance limit (Saleh et al. 2017). Furthermore, in a very recent study, Mlhem et al. (2022) utilized DPF mesh a reinforcement with

Table 7. Composites developed with DPF mesh as a reinforcement.

Polymer Matrix	Filler Type	Fiber Loading Wt.%	Processing Technique	Optimal Fiber Wt.%	Optimal Fiber dimension (mm)	Reference
R-HDPE	Mesh	6	Compression Moulding	6	-	(Aldousiri et al. 2013)
PP-EPDM	Mesh	5, 10, 20, 30	Extrusion & Injection Moulding	-	-	(Eslami-Farsani 2015)
TPS	Mesh	20, 50, 70	Compression Moulding	50	20–30 (length)	(Saleh et al. 2017)
PCL	Mesh	20	Extrusion	20	10.00 (length)	(Dhakal et al. 2018)
RLLDPE	Mesh powder	5	Compression Moulding	-	-	(Alshabanat 2019)
PHB	Mesh	10, 20, 30, 40, 50	Extrusion & Compression molding	-	0.212 (length)	(Mlhem et al. 2022)

polyhydroxybutyrate (PHB) to develop fully biodegradable bio-composite. DPF reduced the overall strength and the density of the composite which is a similar trend to the results obtained in this study due to the weak interfacial bonding of between the polymer and the fiber and the low density of the fiber, respectively. However, the main objective was to investigate the insulation characterizes of the composite (Mlhem et al. 2022). The researchers successfully investigated the effect of DPF loading content but did not evaluate the effect of DPF geometry which plays a vital role in identifying the characteristics of the composites developed due to the non-uniform shape of DPF. In this study the results demonstrate the correlation between DPF geometry and loading content on the characteristics of the developed bio-composite.

Influence of DPF geometry on the microstructure of the composite

Figure 12 shows the SEM microstructure of PLA bio-composite samples with varying DPF size and weight fractions. DPF is a plant fiber that has a hierarchical structure starting from the nano cellulose crystals up to the technical fiber bundles shown in Figure 13b. The technical fiber is made up of bundle of elemental cellulose fibrils which are held together by lignin and hemicellulose. DPF fibrils are characterized by large lumens and small wall thickness creating a cellular structure within the bundle as shown in Figure 13c. The technical fiber has rough surface in the form of hexagonal scales as shown in Figure 13d. While there is poor compatibility between DPF functional groups and PLA, yet the loads can still be transferred from the PLA matrix to the fiber by the interlocking mechanism resulting from the rough fiber surface. The smaller the DPF sieve size the larger the surface area in contact with the PLA matrix, hence better load transfer efficiency and less fiber pullouts are observed. On the other hand, increasing the fiber weight fraction results in voids formation as shown in Figure 13c, due to the high melt viscosity of PLA and difficulty to completely wet the fibers. Under loading the fiber undergoes elastic deformation until debonding from the matrix due to the poor interfacial strength as shown in Figure 13a, further loading results in propagation of the debonding front until the fiber is completely pulled out as shown in Figure 13b.

Conclusion

The utilization of DPF with PLA was successfully achieved using melt-mixing and compression molding processing technologies which could be commercialized for various industrial applications for developing 100% biodegradable bio-composites. The density of the composites shows that lightweight characteristics of the composites that can be developed using DPF. Also, the difference between the theoretical and experimental densities allowed for the calculation of voids fraction within the composites and how it varies depending of DPF size and loading content, which was detrimental in interpreting the composite performance and explaining the effect of void fractions on the interfacial bonding. Void fraction was the highest when utilizing unsieved DPF for developing composites when added at 10–30 wt.%. At 40 wt.%, DPF $\leq 125 \mu\text{m}$ sieve size accounted to have the highest void fraction which is attributed to its low density where there is insufficient PLA to produce a homogenous composite. The void fractions were validated by having the same trend of results as the water absorption test.

DPF utilization affected the physical and mechanical properties of DPF/PLA bio-composites negatively where various DPF sizes has different effects and the increase in DPF content led to a reduction in the mechanical strength of the bio-composite despite the size of DPF. As the DPF content increased within the bio-composites, 10 – 40 wt.%, the TS, WA, and MC % increased due to the hydrophilic nature of DPF which magnified poor fiber-matrix interaction and led to

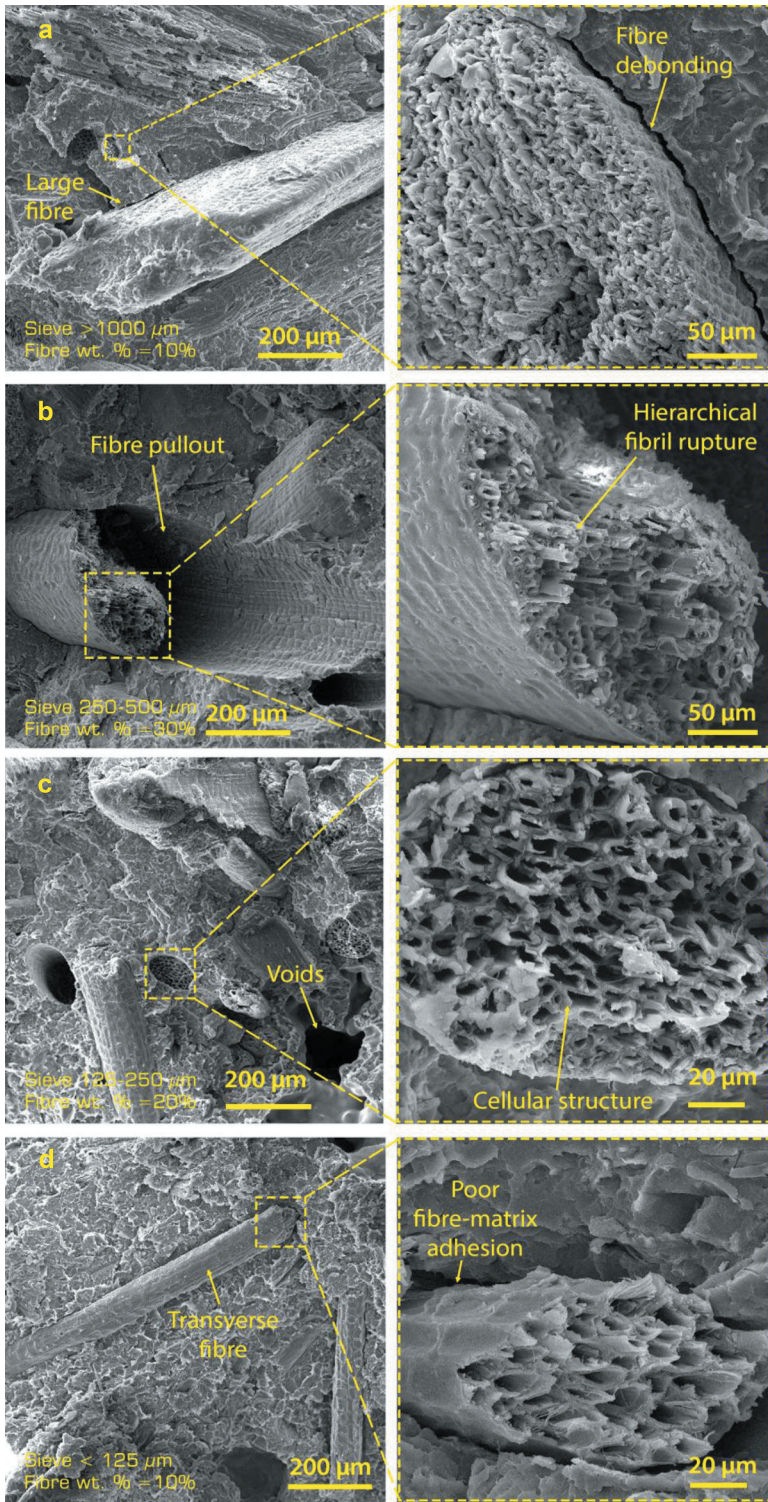


Figure 13. DPF/PLA bio-composites microstructure.

forming more voids within the bio-composite. The same phenomena were shown in testing the flexural strength, tensile strength and impact strength of the bio-composites developed where the strengths decreased with the increase of DPF loading content.

Highlights

- Fully bio-based composite development from DPF agricultural biomass waste and PLA.
- Optimizing DPF/PLA bio-composites with DPF concentration and geometry.
- Establishing correlation of DPF/PLA characteristics and DPF parameters.
- Interfacial bonding properties of DPF/PLA bio-composites.

Disclosure statement

No potential conflict of interest was reported by the author(s).

Funding

This research did not receive any public or private grants and funds.

ORCID

Mohamad Midani  <http://orcid.org/0000-0002-7420-8838>

Evina Katsou  <http://orcid.org/0000-0002-2638-7579>

References

- Abdal-Hay, A., N. P. Gede Suardana, D. Y. Jung, K. S. Choi, and J. K. Lim. 2012. Effect of diameters and alkali treatment on the tensile properties of date palm fiber reinforced epoxy composites. *International Journal of Precision Engineering and Manufacturing* 13 (7):1199–206. doi:10.1007/s12541-012-0159-3.
- Abdul Khalil, H. P. S., A. M. Issam, M. T. Ahmad Shakri, R. Suriani, and A. Y. Awang. 2007. Conventional agro-composites from chemically modified fibres. *Industrial Crops and Products* 26 (3):315–23. doi:10.1016/j.indcrop.2007.03.010.
- Adeniyi, A. G., D. Victoria Onifade, J. O. Ighalo, and A. Samson Adeoye. 2019. A review of coir fiber reinforced polymer composites. *Composites Part B: Engineering* 176 (July):107305. doi:10.1016/j.compositesb.2019.107305.
- Ahmad, A., A. M. Hamed, and K. Al-Kaabi. 2009. Characterization of treated date palm tree fiber as composite reinforcement. *Composites Part B: Engineering* 40 (7):601–06. doi:10.1016/j.compositesb.2009.04.018.
- Aldousiri, B., M. Alajmi, and A. Shalwan. 2013. Mechanical properties of palm fibre reinforced recycled HDPE. *Advances in Materials Science and Engineering*. doi:10.1155/2013/508179.
- Alsaeed, T., B. F. Yousif, and H. Ku. 2013. The potential of using date palm fibres as reinforcement for polymeric composites. *Materials & Design* 43:177–84. doi:10.1016/j.matdes.2012.06.061.
- Alshabanat, M. 2019. Morphological, thermal, and biodegradation properties of LLDPE/treated date palm waste composite buried in a soil environment. *Journal of Saudi Chemical Society* 23 (3):355–64. doi:10.1016/j.jscs.2018.08.008.
- Aly, N. M., H. S. Seddeq, K. Elnagar, and T. Hamouda. 2021. Acoustic and thermal performance of sustainable fiber reinforced thermoplastic composite panels for insulation in buildings. *Journal of Building Engineering* 40:102747. January. doi:10.1016/j.jobbe.2021.102747.
- Amirou, S., A. Zerizer, I. Haddadou, and A. Merlin. 2013. Effects of corona discharge treatment on the mechanical properties of biocomposites from polylactic acid and Algerian date palm Fibres. *Scientific Research and Essays* 8 (21):946–52. doi:10.5897/SRE2013.5507.
- Awad, S., T. Hamouda, M. Midani, Y. Zhou, E. Katsou, and M. Fan. 2021. Date palm fibre geometry and its effect on the physical and mechanical properties of recycled polyvinyl chloride composite. *Industrial Crops and Products* 174 (July):114172. doi:10.1016/j.indcrop.2021.114172.
- Awad, S., Y. Zhou, E. Katsou, Y. Li, and M. Fan. 2020. *A critical review on date palm tree (Phoenix dactylifera L.) fibres and their uses in bio-composites. Waste and biomass valorization*. The Netherlands: Springer. doi:10.1007/s12649-020-01105-2.

- Debeli, D. K., Z. Qin, and J. Guo. 2018. Study on the pre-treatment, physical and chemical properties of ramie fibers reinforced poly (lactic acid) (PLA) biocomposite. *Journal of Natural Fibers* 15 (4):596–610. doi:10.1080/15440478.2017.1349711.
- Del Campo, M., S. Alan, R. R. O. Jorge, M. Arellano, and A. P. F. Aida. 2022. Influence of agro-industrial wastes over the abiotic and composting degradation of polylactic acid biocomposites. *Journal of Composite Materials* 56 (1):43–56. doi:10.1177/00219983211047697.
- Dhokal, H., A. Bourmaud, F. Berzin, F. Almansour, Z. Zhang, D. U. Shah, and J. Beaugrand. 2018. Mechanical properties of leaf sheath date palm fibre waste biomass reinforced polycaprolactone (PCL) biocomposites. *Industrial Crops and Products* 126:394–402. doi:10.1016/j.indcrop.2018.10.044.
- Dong, Y., A. Ghataura, H. Takagi, H. J. Haroosh, A. N. Nakagaito, and K. Tak Lau. 2014. Polylactic acid (PLA) biocomposites reinforced with coir fibres: Evaluation of mechanical performance and multifunctional properties. *Composites: Part A, Applied Science and Manufacturing* 63:76–84. doi:10.1016/j.compositesa.2014.04.003.
- Elseify, L. A., M. Midani, A. H. Hassanin, T. Hamouda, and R. Khiari. 2020. Long textile fibres from the midrib of date palm: Physicochemical, morphological, and mechanical properties. *Industrial Crops and Products* 151: 112466. September 2019. doi:10.1016/j.indcrop.2020.112466.
- Elseify, L. A., M. Midani, L. A. Shihata, and H. El-Mously. 2019. Review on cellulosic fibers extracted from date palms (*Phoenix dactylifera* L.) and their applications. *Cellulose*. Springer Netherlands. doi:10.1007/s10570-019-02259-6.
- Eslami-Farsani, R. 2015. Effect of fiber treatment on the mechanical properties of date palm fiber reinforced PP/EPDM composites. *Advanced Composite Materials* 24 (1):27–40. doi:10.1080/09243046.2013.871177.
- Foruzanmehr, M., P. Y. Vuillaume, S. Elkoun, and M. Robert. 2016. Physical and mechanical properties of PLA composites reinforced by TiO₂ grafted flax fibers. *Materials & Design* 106:295–304. doi:10.1016/j.matdes.2016.05.103.
- Hamouda, T., and N. M. Aly. 2020. Date palm fiber composites for automotive applications. In *Date palm fiber composites*, ed. M. Midani, N. Saba, and O. Y. Allothman, 387–405. Singapore: Springer. doi:10.1007/978-981-15-9339-0_14.
- Hamouda, T., and A. H. Hassanin. 2020. Date palm fiber composites: Mechanical testing and properties. In *Date palm fiber composite*, ed. M. Midani, N. Saba, and O. Y. Allothman, 257–66. Singapore: Springer. doi:10.1007/978-981-15-9339-0_9.
- Hamouda, T., A. H. Hassanin, A. Kilic, Z. Candan, and M. Safa Bodur. 2017. Hybrid composites from coir fibers reinforced with woven glass fabrics: Physical and mechanical evaluation. *Polymer Composites* 38 (10):2212–20. doi:10.1002/pc.23799.
- Hassanin, A. H., T. Hamouda, Z. Candan, A. Kilic, and T. Akbulut. 2016. Developing high-performance hybrid green composites. *Composites Part B: Engineering* 92:384–94. doi:10.1016/j.compositesb.2016.02.051.
- Herrera-Franco, P. J., and A. Valadez-González. 2004. Mechanical properties of continuous natural fibre-reinforced polymer composites. *Composites: Part A, Applied Science and Manufacturing* 35 (3):339–45. doi:10.1016/j.compositesa.2003.09.012.
- Huda, M. S., L. T. Drzal, A. K. Mohanty, and M. Misra. 2008. Effect of fiber surface-treatments on the properties of laminated biocomposites from poly(lactic acid) (PLA) and kenaf fibers. *Composites Science and Technology* 68 (2):424–32. doi:10.1016/j.compscitech.2007.06.022.
- Jia, W., R. H. Gong, and J. H. Paul. 2014. Poly (lactic acid) fibre reinforced biodegradable composites. *Composites Part B: Engineering* 62:104–12. doi:10.1016/j.compositesb.2014.02.024.
- Lahouioui, M., R. Ben Arfi, M. Fois, L. Ibos, and A. Ghorbal. 2019. Investigation of fiber surface treatment effect on thermal, mechanical and acoustical properties of date palm fiber-reinforced cementitious composites. *Waste and Biomass Valorization* 11 (8):0123456789. doi:10.1007/s12649-019-00745-3.
- Madurwar, M. V., R. V. Ralegaonkar, and S. A. Mandavgane. 2013. Application of agro-waste for sustainable construction materials: A review. *Construction and Building Materials* 38:872–78. doi:10.1016/j.conbuildmat.2012.09.011.
- Matuana, L. M., R. T. Woodhams, J. J. Balatinez, and C. B. Park. 1998. Influence of interfacial interactions on the properties of PVC/cellulosic fiber composites. *Polymer Composites* 19 (4):446–55. doi:10.1002/pc.10119.
- Mittal, V., R. Saini, and S. Sinha. 2016. Natural fiber-mediated epoxy composites - A review. *Composites Part B: Engineering* 99:425–35. doi:10.1016/j.compositesb.2016.06.051.
- Milhem, A., B. Abu-Jdayil, T. Tong-Earn, and M. Iqbal. 2022. Sustainable heat insulation composites from date palm fibre reinforced poly (β -hydroxybutyrate). *Journal of Building Engineering* 54:104617. doi:10.1016/j.jobee.2022.104617.
- Oushabi, A., S. Sair, F. Oudrhiri Hassani, Y. Abboud, O. Tanane, and A. El Bouari. 2017. The effect of alkali treatment on mechanical, morphological and thermal properties of Date Palm Fibers (DPFs): Study of the interface of DPF-polyurethane composite. *South African Journal of Chemical Engineering* 23 (June):116–23. doi:10.1016/j.sajce.2017.04.005.
- Ozerkan, N. G., B. Ahsan, S. Mansour, and S. R. Iyengar. 2013. Mechanical performance and durability of treated palm fiber reinforced mortars. *International Journal of Sustainable Built Environment* 2 (2):131–42. doi:10.1016/j.ijbsbe.2014.04.002.

- Pickering, K. L., G. W. Beckermann, S. N. Alam, and N. J. Foreman. 2007. Optimising industrial hemp fibre for composites. *Composites: Part A, Applied Science and Manufacturing* 38 (2):461–68. doi:10.1016/j.compositesa.2006.02.020.
- Puglia, D., J. Biagiotti, and J. M. Kenny. 2004. A review on natural fibre-based composites - Part II: Application of natural reinforcements in composite materials for automotive industry. *Journal of Natural Fibers* 1 (3):23–65. doi:10.1300/J395v01n03_03.
- Radzi, A. M., S. M. Sapuan, M. Jawaid, and M. R. Mansor. 2019. Water absorption, thickness swelling and thermal properties of Roselle/sugar palm fibre reinforced thermoplastic polyurethane hybrid composites. *Journal of Materials Research and Technology* 8 (5):3988–94. doi:10.1016/j.jmrt.2019.07.007.
- Rana, A. K., A. Mandal, and S. Bandyopadhyay. 2003. Short jute fiber reinforced polypropylene composites: Effect of compatibiliser, impact modifier and fiber loading. *Composites Science and Technology* 63 (6):801–06. doi:10.1016/S0266-3538(02)00267-1.
- Rao, K. M. M., and K. M. Rao. 2007. Extraction and tensile properties of natural fibers: Vakka, date and bamboo. *Composite Structures* 77 (3):288–95. doi:10.1016/j.compstruct.2005.07.023.
- Said, A., Y. Zhou, E. Katsou, and M. Fan. 2020. Polymer matrix systems used for date palm composite reinforcement. In *Date palm fiber composite*, ed. M. Midani, N. Saba, and O. Y. Alothman, 119–59. Singapore: Springer. doi:10.1007/978-981-15-9339-0_4.
- Saleh, M. A., M. H. Al Haron, A. A. Saleh, and M. Farag. 2017. Fatigue behavior and life prediction of biodegradable composites of starch reinforced with date palm fibers. *International Journal of Fatigue* 103:216–22. doi:10.1016/j.ijfatigue.2017.06.005.
- Shakeri, A., and A. Ghasemian. 2010. Water absorption and thickness swelling behavior of polypropylene reinforced with hybrid recycled newspaper and glass fiber. *Applied Composite Materials* 17 (2):183–93. doi:10.1007/s10443-009-9111-9.
- Siakeng, R., M. Jawaid, M. Asim, and S. Siengchin. 2020. Accelerated weathering and soil burial effect on biodegradability, colour and texture of coir/pineapple leaf fibres/PLA biocomposites. *Polymers* 12 (2):2. doi:10.3390/polym12020458.
- Swain, P. T. R., and S. Biswas. 2013. Physical and mechanical behavior of Al₂O₃ filled jute fiber reinforced epoxy composites. *International Journal of Current Engineering and Technology* 2 (2):67–71. doi:10.14741/ijcet/spl.2.2014.13.
- Taha, I., L. Steuernagel, and G. Ziegmann. 2006. Chemical modification of date palm mesh fibres for reinforcement of polymeric materials. Part I examination of different cleaning methods. *Polymers and Polymer Composites* 14 (8):767–78. doi:10.1177/096739110601400802.
- Tahri, I., I. Ziegler Devin, J. Ruelle, C. Segovia, and N. Brosse. 2016. Extraction and characterization of fibers from palm tree. *BioResources* 11 (3):3. doi:10.15376/biores.11.3.7016-7025.
- Thwe, M. M., and K. Liao. 2002. Effects of environmental aging on the mechanical properties of bamboo-glass fiber reinforced polymer matrix hybrid composites. *Composites - Part A: Applied Science and Manufacturing* 33 (1):43–52. doi:10.1016/S1359-835X(01)00071-9.
- Trotignon, J. P., B. Sanschagrin, M. Piperaud, and J. Verdu. 1982. Mechanical properties of mica-reinforced polypropylene composites. *Polymer Composites* 3 (4):230–38. doi:10.1002/pc.750030409.
- Zhou, F., G. Cheng, and B. Jiang. 2014. Effect of silane treatment on microstructure of sisal fibers. *Applied Surface Science* 292:806–12. doi:10.1016/j.apsusc.2013.12.054.